Journal of Physics B: Atomic,
Molecular and Optical Physics

PAPER • **OPEN ACCESS**

Under-threshold RABBITT in argon

To cite this article: Anatoli S Kheifets 2023 *J. Phys. B: At. Mol. Opt. Phys.* **56** 095201

OPEN ACCESS
IOP Publishing
Journal of Physics B: Atomic, Molecular and Optical Physics
J. Phys. B: At. Mol. Opt. Phys. **56** (2023) 095201 (6pp)
https://doi.org/10.1088/1361-6455/acc6aa

Under-threshold RABBITT in argon

Anatoli S Kheifets

Fundamental and Theoretical Physics, Research School of Physics, The Australian National University, Canberra 2601, Australia

E-mail: a.kheifets@anu.edu.au

Received 3 January 2023, revised 8 March 2023
Accepted for publication 22 March 2023
Published 4 April 2023

Abstract

The process of reconstruction of attosecond bursts by beating of two-photon transitions (RABBITT) can involve a transition from under the ionization threshold. Such an under-threshold RABBITT (or uRABBITT) was demonstrated experimentally and analyzed theoretically in He and Ne. In the present work, we explore an analogous process in the argon atom. The uRABBITT in Ar reveals the familiar physical effects: a phase transition across the threshold and the symmetry modification of the photoelectron momentum distribution. It can also be used for mapping the electronic structure of the target atom bound states.

Keywords: under-threshold, RABBITT, argon

(Some figures may appear in colour only in the online journal)

1. Introduction

Resolving photoemission in time was one of the most significant achievements of atomic and molecular physics in the past decade. The process of reconstruction of attosecond bursts by beating of two-photon transitions (RABBITT) (Paul *et al* 2001, Mairesse *et al* 2003) has been credited with this achievement. Starting with the pioneering work by Klünder *et al* (2011), RABBITT has been widely used for time resolution of photoemission from atoms, molecules and condensed matter (see Pazourek *et al* 2015, Borrego-Varillas *et al* 2022 and Kheifets 2023 for reviews). The RABBITT process involves two ionizing transitions driven by odd harmonics of the fundamental laser frequency $\Omega_{2q\pm1} = (2q \pm 1)\omega$ supplemented by absorption or emission of one ω photon. This two-photon ionization process creates an even order sideband SB_{2q} in the photoelectron spectrum. The population of this sideband oscillates as the time delay between the Ω and ω laser pulses varies:

$$S_{2q}(\tau) = A + B\cos[2\omega\tau - C]\ . \tag{1}$$

Here A and B are the magnitude parameters whereas C is the RABBITT phase which can be converted to the atomic time delay $\tau_a = C/(2\omega)$ (Véniard *et al* 1996, Dahlström *et al* 2012). In a conventional RABBITT, both the $\pm\omega$ ionization processes involve transitions in the continuum. However, when $\Omega_{2q-1} < I_p$, the $+\omega$ transition should proceed from under the threshold. This discrete-to-continuum transition is strongly promoted by an overlap with a bound state of the target atom. Such an under-threshold RABBITT (or uRABBITT for brevity) was observed experimentally in He (Swoboda *et al* 2010) and Ne (Villeneuve *et al* 2017). A detailed theoretical study (Kheifets and Bray 2021) revealed the uRABBITT phase transition across the ionization threshold. By sharpening the energy resolution, the uRABBITT process was shown to map faithfully the target atom bound states (Kheifets 2021). Both the experiment (Villeneuve *et al* 2017) and theory (Kheifets 2022) revealed a strong modification of the photoelectron momentum distribution across the ionization threshold. Very recently, the rainbow RABBITT technique was used to study the uRABBITT process in He (Autuori *et al* 2022, Drescher *et al* 2022, Neoričić *et al* 2022). In these works, the base frequency of a wideband infrared (IR) pulse was fixed while narrow bandpass filters were used to scan the photoelectron spectrum over the resonance.

In the present work, we uncover the uRABBITT process in the argon atom which was not reported previously. Unlike the two other atoms, He and Ne, the fundamental laser frequency

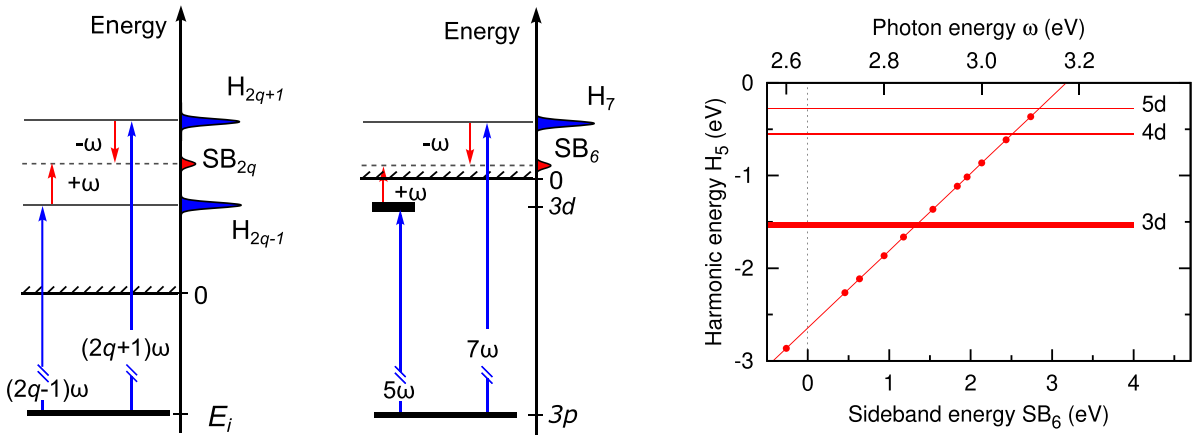

Figure 1. Left: schematic of a generic RABBITT process. Center: analogous schematic of the uRABBITT on Ar at 435 nm. Right: energy positions of the sideband SB_6 and the primary harmonic peak H_5 as the functions of the photon energy ω. The uRABBITT transition occurs when H_5 passes the $3d$ energy level while SB_6 is above the ionization threshold. The thickness of the lines marking bound state energy levels reflects the corresponding oscillator strengths.

should be doubled changing the wavelength from the 800 nm to 400 nm range[1]. By doing so, the transition from the ground $3p$ to the excited $3d$ bound state can be facilitated with the fifth harmonic of the fundamental frequency as illustrated graphically in figure 1. Accordingly, the sideband SB_6 undergoes the uRABBITT phase transition in the photon energy range $2.8 \leqslant \omega \leqslant 2.9$ eV ($442 \geqslant \lambda \geqslant 427$ nm). This transition is accompanied by a noticeable modification of the photoelectron momentum distribution. Both effects can be used as convenient tools for probing and mapping the target atom electronic structure.

The rest of the paper is organized in the following way. In section 2 we give a brief outline of our computational methods. Section 3 contains our main numerical results divided into angular resolved and angular integrated spectra. We conclude in section 4 by outlining further extensions of the present work.

2. Methods

We follow closely our previous works (Bray *et al* 2018, Kheifets and Bray 2021). In brief, we solve numerically the time-dependent Schrödinger equation (TDSE) in a single-active electron approximation[2]:

$$i\partial\Psi(\boldsymbol{r})/\partial t = \left[\hat{H}_{\rm atom} + \hat{H}_{\rm int}(t)\right]\Psi(\boldsymbol{r})\ . \tag{2}$$

Here the radial part of the atomic Hamiltonian

$$\hat{H}_{\rm atom}(r) = -\frac{1}{2}\frac{d^2}{dr^2} + \frac{l(l+1)}{2r^2} + V(r) \tag{3}$$

contains an effective one-electron potential $V(r)$. This potential is obtained by localizing the non-local Hartree–Fock (HF) potential as prescribed by Wendin and Starace (1978). Thus obtained localized (LHF) potential returns the bound state energies listed in table 1.

The interaction Hamiltonian $\hat{H}_{\rm int}(t)$ in equation (2) is written in the velocity gauge

$$\hat{H}_{\rm int}(t) = \boldsymbol{A}(t)\cdot\hat{\boldsymbol{p}}\ ,\ \ \boldsymbol{A}(t) = -\int_0^t \boldsymbol{E}(t')\,{\rm d}t'\ . \tag{4}$$

The vector potential represents the linearly polarized XUV and IR fields. The extreme ultraviolet (XUV) field is taken as an attosecond pulse train (APT) containing 41 pulselets of the opposite polarities and 30 as duration. The total width of the APT is about 30 fs whereas that of the IR pulse is close to 15 fs. The APT is centered at $\omega_x = 15\omega$ and its spectral width $\Gamma \simeq 0.2$ eV. The base frequency ω is incremented with a typical step of 0.02 eV. The IR and XUV intensities are both 1×10^{10} W cm^{-2}. Solution of equation (2) is sought with the spherical-coordinate implicit derivatives method implemented in the computer code by Morales *et al* (2016). The photoelectron momentum distribution (PMD) was obtained by projecting the time-dependent wave function at the end of the propagation on the basis of the plane waves

$$P_m(\boldsymbol{k}) = \left|\langle\varphi_{\boldsymbol{k}}(r)|\Psi_{nlm}(\boldsymbol{r}, t\to\infty)|\rangle\right|^2\ . \tag{5}$$

Here the indexes n,l,m denote the initial atomic bound state (the Ar $3p_m$ ground state). The photoelectron momentum $\boldsymbol{k}$ is defined in the Cartesian plane in which the $\hat{z}$ axis is aligned with the joint polarization direction of the XUV and IR pulses. Projection on the $k_y = 0$ plane $P(k_x, k_z)$ serves to determine the angular symmetry of the main harmonic peaks and the sidebands. The angular integrated photoelectron spectrum is obtained as

$$P_m(E) = \int k^2 {\rm d}\Omega_k\, P_m(\boldsymbol{k})\ ,\ \ E = k^2/2\ . \tag{6}$$

[1] We note that 400 nm radiation belongs to the visible spectrum but we keep using the XUV + IR nomenclature to remain consistent with majority of RABBITT works.

[2] Here and throughout, we use the atomic units (a.u.) by setting $e = m = \hbar = 1$.

Table 1. Bound state energies of Ar from the HF and LHF calculations are compared with recommended NIST values (Kramida *et al* 2014). The optical oscillator strength are returned by the ATOM program suite (Amusia and Chernysheva 1997).

Term	nl	Energy, atomic units			Oscillator strengths
		HF	LHF	NIST	
$2p^6(^1S_0)$	$3p$	−0.591	−0.5803	−0.5791	
$2p^5(^2P_{1/2})$	$3d$	−0.0585	−0.0564	−0.0567	0.1837
	$4d$	−0.0331	−0.3176	−0.0296	0.0907
	$5d$	−0.0210	−0.0203	−0.0240	0.0481
	$4s$	−0.1408	−0.1437	−0.1482	0.3125
	$5s$	−0.0591	−0.0602	−0.0558	0.0295

The sideband population is determined as

$$S_{2q} = \sum_m \int_{E_{2q}-\Gamma}^{E_{2q}+\Gamma} \mathrm{d}E\, P_m(E) \;\;,\;\; E_{2q} = 2q\omega - I_p. \tag{7}$$

The XUV/IR time delay τ is implicit in equations (5)–(7) but not shown for brevity of notations.

3. Results

3.1. Angular resolved photoelectron spectra

The PMD $P(k_x, k_z)$ projected on the $k_y = 0$ plane is exhibited in figure 2. The top row of panels shows the primary harmonic peaks H7, 9 and 11 corresponding to the Ar atom prepared in the $3p_m$ initial state ($m = 0$ – left and $m = 1$ – center) or summed over m (right). The primary harmonics display clearly the Y_{2m} angular symmetry as illustrated in the bottom row of panels. This supports the Fano (1985) propensity rule which favors strongly the discrete-continuous transitions with an increase of the angular momentum. The same applies to the discrete–discrete transitions as is seen from the optical oscillator strength at comparable energies (see table 1). When summed over m, the $m = 0$ symmetry still persists especially in the H7 harmonic peak. In the middle row of panels, the sidebands SB6, 8 and 10 are displayed whereas the primary harmonic peaks are masked for clarity. The sidebands show the Y_{1m} angular symmetry. This is in sharp contrast to the analogous spectra of the Ne atom in the initial $2p_m$ state which demonstrate the Y_{3m} symmetry (Villeneuve *et al* 2017, Kheifets 2022). It was suggested by Busto *et al* (2019) that the same angular momentum increase propensity holds for the transitions in the continuum. The Ar $3p_m$ case does not satisfy this rule. Summation over m smooths the angular anisotropy of the sidebands except for SB6 which still retains the $3p_{m=0}$ angular character.

3.2. Angular integrated spectra

The spectra shown in figure 2 correspond to the XUV/IR time delay $\tau = 0$. Explicit τ dependence is shown in figure 3 which displays the RABBITT traces recorded at the two photon energies ω of 2.8 eV (left) and 2.9 eV (right). These traces are formed by vertical stacks of several angular-integrated spectra taken at various XUV/IR time delays. The primary harmonic features in these spectra are masked for better clarity. The SB's oscillate with time delay as prescribed by equation (1). The SB centers are joined by solid lines to show more clearly the SB dispersion. While this dispersion is very weak for SB8 and above, the SB6 falls out from this nearly perfect line up. It deviates visibly to the left at $\omega = 2.8$ eV and to the right at $\omega = 2.9$ eV.

To highlight this deviation more clearly, we plot in figure 4 the RABBITT phase parameters C for the three lowest sidebands SB6, 8 and 10. The left panel displays the C dependence on the photoelectron energy E whereas the right panel shows the photon energy ω dependence. While the C parameters of the SB8 and 10 are essentially flat, SB6 shows a rapid oscillation of the C parameter in the left panel. The nature of this oscillation can be explained by a simple perturbation theory model introduced by Drescher *et al* (2022). According to this model, the phase of the two-photon transition amplitude from the ground g to the final f states near the resonance behaves as

$$\arg\left[a_{g\to f}^{(\mathrm{near})\mathrm{res}}\right] \to \begin{cases} \pi/2 & \omega < \omega_{ng} \\ 3\pi/2 & \omega > \omega_{ng} \end{cases} \tag{8}$$

Here ω_{ng} is the transition frequency connecting the ground state g and an intermediate discrete state n. To visualize this phase shift by one unit of π, we add it to the RABBITT phase for $\omega \leqslant 2.9$ eV. This way the phase dependence on the photon frequency becomes smooth and shows a very distinct RABBITT–uRABBITT phase transition.

Not only does the C parameter oscillate in SB6. The corresponding B parameter also shows an oscillatory structure. Figure 5 lines up the C and B parameters side-by-side for the lowest SB6, 8 and 10. As in figure 4, the corresponding C and B parameters are flat for SB8 and 10 whereas SB6 displays well synchronized oscillations in the C and B parameters. The B parameter peaks very sharply when the submerged harmonic H5 crosses the discrete $3d$ and $4d$ levels as can be seen from the energy diagram exhibited in the right panel of figure 1. We could anticipate a similar oscillation of the phase C and magnitude B parameters near the discrete $5d$ and higher states. But we do not observe it in the present simulation either because our photon energy scan stops at 3.1 eV or we do not have a sufficient energy resolution.

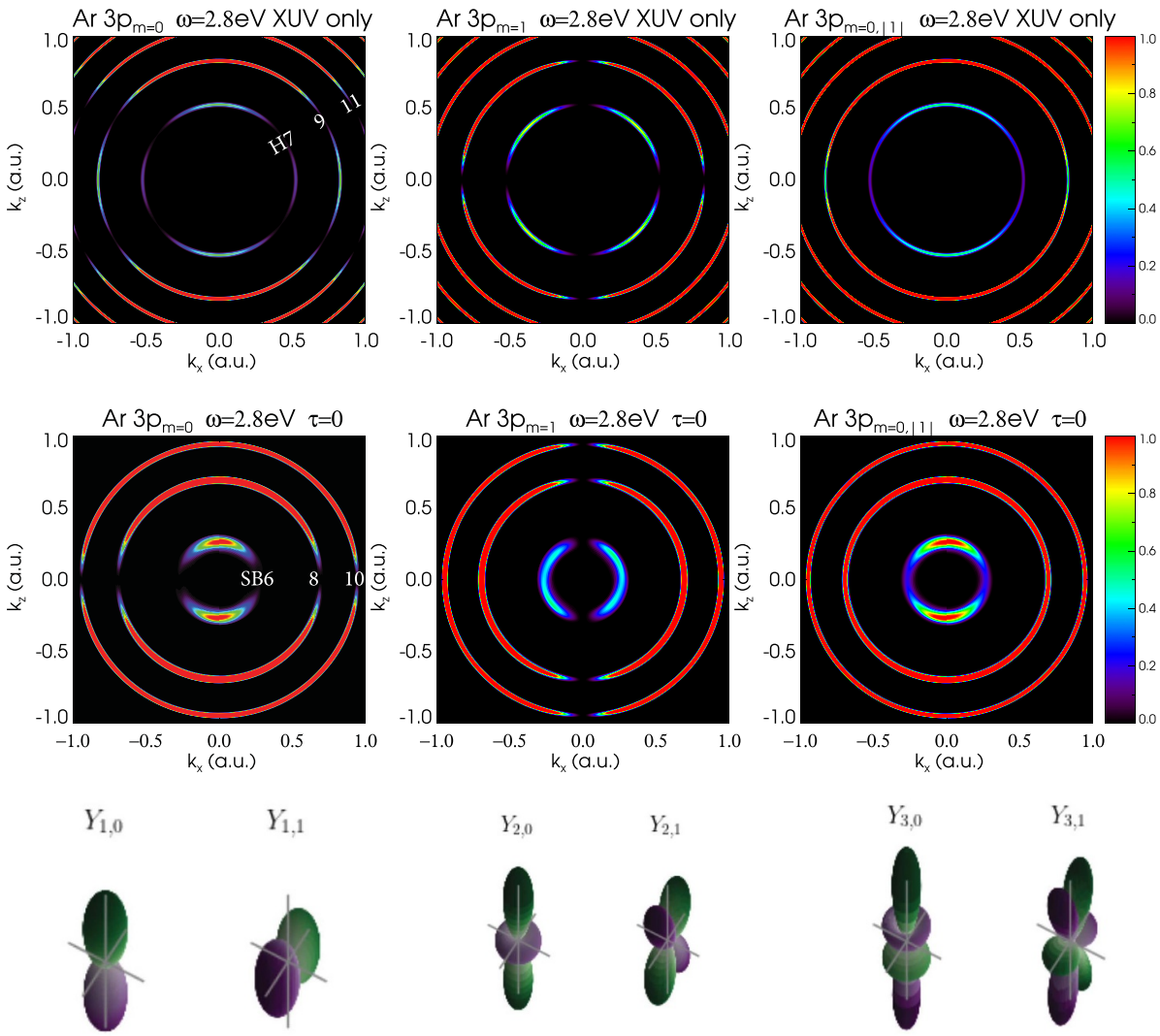

Figure 2. Photoelectron momentum distribution $P(k_x, k_z)$ projected on the $k_y = 0$ plane corresponding to the initial $3p_m$ initial state with $m = 0$ (left), $m = 1$ (center) or summed over m (right). The top row corresponds to XUV only spectra which visualize the primary harmonic peaks. The central row displays the sidebands originated from two-photon ionization at the XUV/IR time delay $\tau = 0$. The primary harmonic peaks are masked for clarity. The bottom row shows the symmetry of the corresponding spherical harmonics.

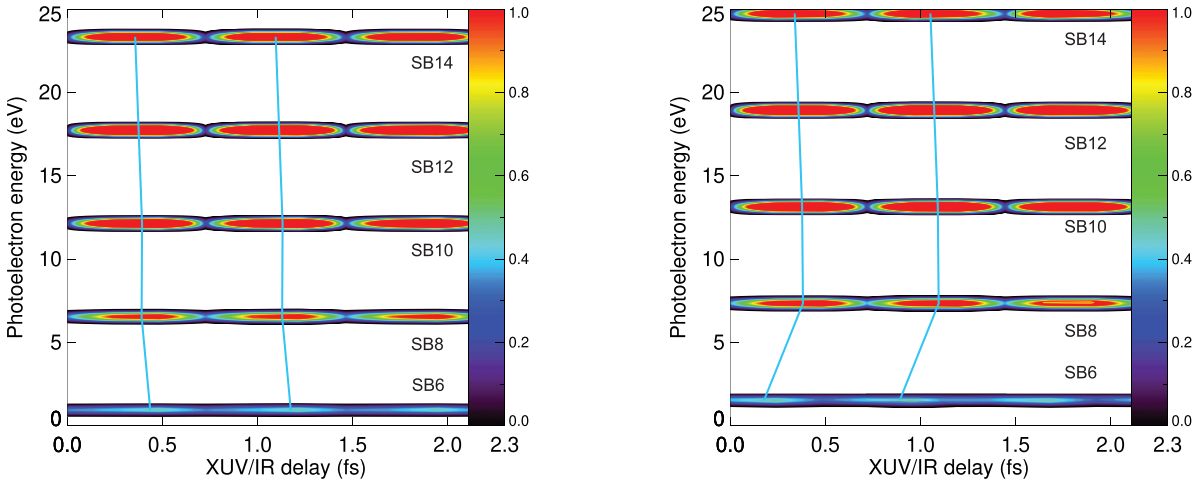

Figure 3. RABBITT traces of Ar at $\omega = 2.8$ eV (left) and $\omega = 2.9$ eV (right). The SB centers are joined by the solid blue lines to guide the eye. The main harmonic peaks are masked for clarity.

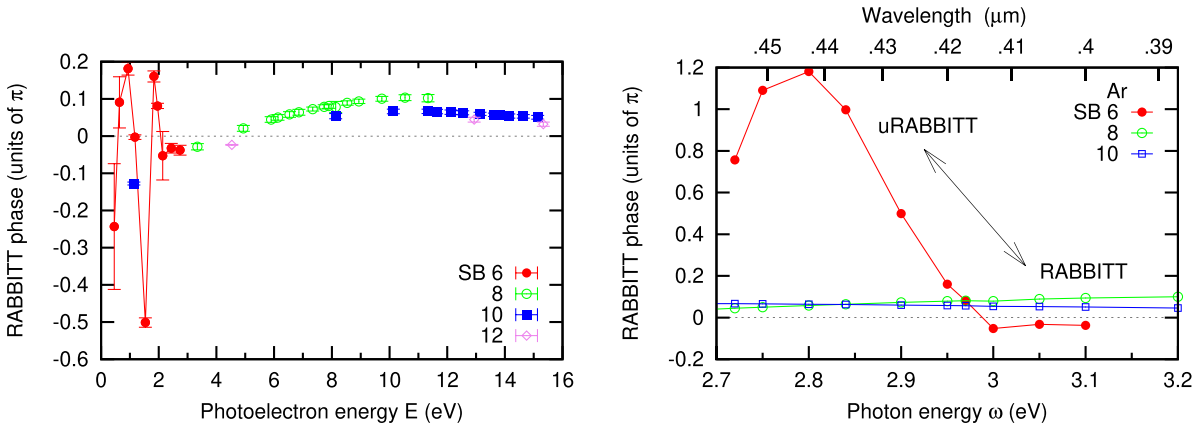

Figure 4. RABBITT phase of Ar as a function of the photoelectron energy E (left) and base photon frequency ω (right). The phase at the right plot is augmented by one unit of π for $\omega < 2.9$ eV.

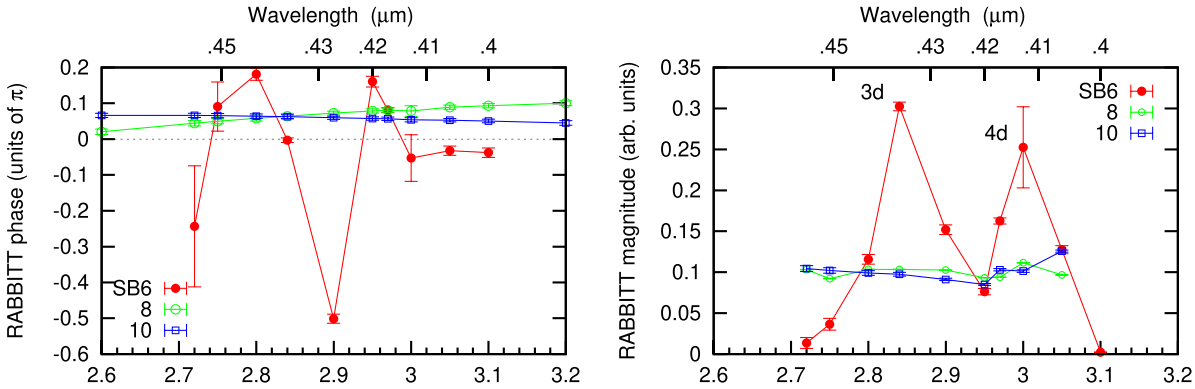

Figure 5. RABBITT phase C (left) and magnitude B (right) parameters in Ar as functions of the photon frequency ω. The top scale shows the corresponding wavelength.

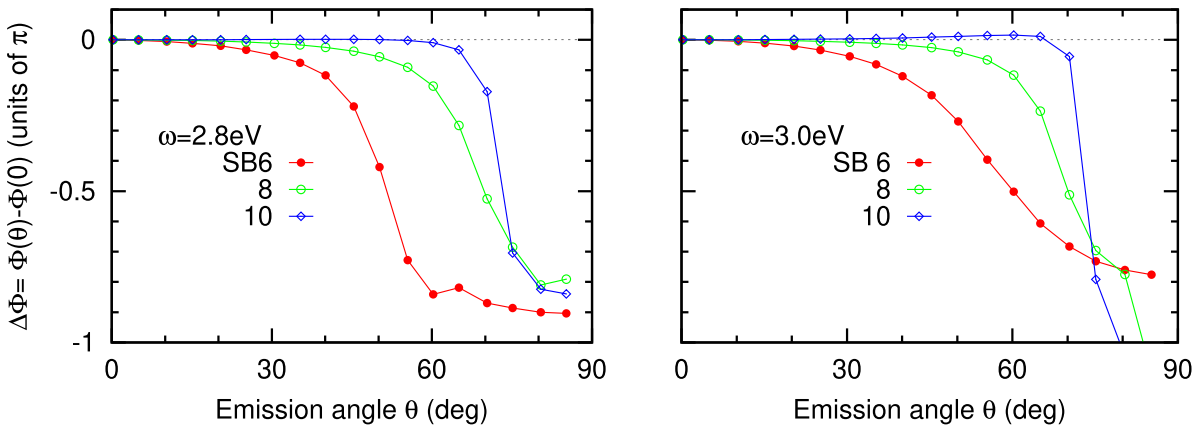

Figure 6. Angular variation of the RABBITT phase for SB6, 8 and 10 relative to the polarization direction $\theta = 0$ at $\omega = 2.8$ eV (left) and $\omega = 3.0$ eV (right).

The uRABBITT phase transition in SB6 is also reflected in the angular dependence of the C parameter when the photoelectron emission angle θ is taken away from the polarization direction corresponding to $\theta = 0$. This dependence is shown in figure 6 for the two photon energies $\omega = 2.8$ eV (left) and $\omega = 3$ eV (right). The 'normal' SB8 and 10 show very little angular dependence in their C parameters below the magic angle $\theta_m = 54.7°$ corresponding to the kinematic node of Y_{20}. At the same time, the C parameter of SB6 starts deviation from the polarization direction at considerably smaller photoelectron emission angles.

4. Conclusion

We demonstrate the clear signatures of the uRABBITT process in the argon atom which was discovered earlier in the He

and Ne atoms. The present demonstration of uRABBITT in Ar is first of its kind. Due to peculiarity of the bound state structure, uRABBITT in Ar occurs at the fundamental frequency in the 400 nm wavelength range. This range can be reached by doubling the photon frequency of the most commonly used 800 nm Chirped pulse amplification lasers. The uRABBITT in Ar is facilitated by the harmonic peak H5 crossing the 3*d* and 4*d* energy levels. This is accompanied by a strong oscillation of the RABBITT phase *C* and magnitude *B* parameters of SB6 whereas the analogous parameters for higher order sidebands remain essentially flat. The SB symmetry analysis shows a clear violation of the propensity rule suggesting an angular momentum increase in the continuum transitions. This rule holds for the analogous transitions in the Ne atom.

The observations made in the present work suggest an universality of the uRABBITT process. Its direct link with the target atom electronic structure allows to map the binding energies and oscillator strengths for the discrete transitions. The same technique can be applied to more complex targets such as molecules. We hope that our findings will stimulate these studies.

Data availability statement

All data that support the findings of this study are included within the article (and any supplementary files).

Acknowledgments

The author thanks Daniel Hammerland for many stimulating discussions. Resources of the National Computational Infrastructure facility have been used in this work.

ORCID iD

Anatoli S Kheifets https://orcid.org/0000-0001-8318-9408

References

Amusia M I and Chernysheva L V 1997 *Computation of Atomic Processes: A Handbook for the Atom Programs* (Bristol: Institute of Physics Publishing Ltd)

Autuori A *et al* 2022 Anisotropic dynamics of two-photon ionization: an attosecond movie of photoemission *Sci. Adv.* **8** eabl7594

Borrego-Varillas R, Lucchini M and Nisoli M 2022 Attosecond spectroscopy for the investigation of ultrafast dynamics in atomic, molecular and solid-state physics *Rep. Prog. Phys.* **85** 066401

Bray A W, Naseem F and Kheifets A S 2018 Simulation of angular-resolved RABBITT measurements in noble-gas atoms *Phys. Rev.* A **97** 063404

Busto D *et al* 2019 Fano's propensity rule in angle-resolved attosecond pump-probe photoionization *Phys. Rev. Lett.* **123** 133201

Dahlström J, Guénot D, Klünder K, Gisselbrecht M, Mauritsson J, Huillier A L, Maquet A and Taïeb R 2012 Theory of attosecond delays in laser-assisted photoionization *Chem. Phys.* **414** 53–64

Drescher L, Witting T, Kornilov O and Vrakking M J J 2022 Phase dependence of resonant and antiresonant two-photon excitations *Phys. Rev.* A **105** L011101

Fano U 1985 Propensity rules: an analytical approach *Phys. Rev.* A **32** 617–8

Kheifets A 2021 Revealing the target electronic structure with under-threshold RABBITT *Atoms* **9** 66

Kheifets A S 2022 Symmetry analysis of the photoelectron continuum in two-photon XUV + IR ionization *Phys. Rev.* A **105** 013114

Kheifets A S 2023 Wigner time delay in atomic photoionization *J. Phys. B: At. Mol. Opt. Phys.* **56** 022001

Kheifets A S and Bray A W 2021 RABBITT phase transition across the ionization threshold *Phys. Rev.* A **103** L011101

Klünder K *et al* 2011 Probing single-photon ionization on the attosecond time scale *Phys. Rev. Lett.* **106** 143002

Kramida A, Ralchenko Y and Reader J (NIST ASD Team) 2014 *NIST Atomic Spectra Database (Ver. 5.2)* (Gaithersburg, MD: National Institute of Standards and Technology) (available at: http://physics.nist.gov/asd) (Accessed 30 June 2015)

Mairesse Y *et al* 2003 Attosecond synchronization of high-harmonic soft x-rays *Science* **302** 1540–3

Morales F, Bredtmann T and Patchkovskii S 2016 iSURF: a family of infinite-time surface flux methods *J. Phys. B: At. Mol. Opt. Phys.* **49** 245001

Neoričić L *et al* 2022 Resonant two-photon ionization of helium atoms studied by attosecond interferometry *Front. Phys.* **10** 964586

Paul P M, Toma E S, Breger P, Mullot G, Augé F, Balcou P, Muller H G and Agostini P 2001 Observation of a train of attosecond pulses from high harmonic generation *Science* **292** 1689–92

Pazourek R, Nagele S and Burgdörfer J 2015 Attosecond chronoscopy of photoemission *Rev. Mod. Phys.* **87** 765

Swoboda M, Fordell T, Klünder K, Dahlström J M, Miranda M, Buth C, Schafer K J, Mauritsson J, L'Huillier A and Gisselbrecht M 2010 Phase measurement of resonant two-photon ionization in helium *Phys. Rev. Lett.* **104** 103003

Véniard V, Taïeb R and Maquet A 1996 Phase dependence of $(n+1)$-color $(n>1)$ ir-uv photoionization of atoms with higher harmonics *Phys. Rev.* A **54** 721–8

Villeneuve D M, Hockett P, Vrakking M J J and Niikura H 2017 Coherent imaging of an attosecond electron wave packet *Science* **356** 1150–3

Wendin G and Starace A F 1978 Perturbation theory in a strong-interaction regime with application to 4d-subshell spectra of Ba and La *J. Phys. B: At. Mol. Phys.* **11** 4119